Sizing and operation co-optimization strategy for flexible traction power supply system

Zhang, Shanshan; Yang, Shaobing; Liu, Qiujiang; Hu, Bin; Zhang, Junting; Guerrero, Josep

Published in:
IET Renewable Power Generation

DOI (link to publication from Publisher):
10.1049/rpg2.12626

Publication date:
2023

Document Version
Publisher's PDF, also known as Version of record

IET Renewable Power Generation

Special Issue Call for Papers

Be Seen. Be Cited.
Submit your work to a new IET special issue

Connect with researchers and experts in your field and share knowledge.

Be part of the latest research trends, faster.

Read more

The Institution of Engineering and Technology

Received: 29 June 2022 | Revised: 22 September 2022 | Accepted: 13 October 2022

IET Renewable Power Generation

DOI: 10.1049/rpg2.12626

The Institution of Engineering and Technology WILEY

ORIGINAL RESEARCH

Sizing and operation co-optimization strategy for flexible traction power supply system

Shanshan Zhang[1] | **Shaobing Yang**[1] | **Qiujiang Liu**[1] | **Bin Hu**[2] | **Junting Zhang**[1] | **Josep Guerrero**[3]

[1]Electrical Engineering Department, Beijing Jiaotong University, Beijing, P. R. China

[2]Electrical Engineering Department, Zhejiang University, Hangzhou, P. R. China

[3]Energy Department, Aalborg University, Aalborg, Denmark

Correspondence
Shaobing Yang, Electrical Engineering Department, Beijing Jiaotong University, No. 3 Shangyuancun, Beijing, P. R. China.
Email: shbyang@bjtu.edu.cn

Funding information
National Key Research and Development Program of China, Grant/Award Number: 2021YFB2601303

Abstract

Dispatchable energy storage system (ESS) plays a critical role in the smart grid through energy shift and power support. However, it exhibits different operational strategies and economic benefits in different application scenarios due to its inherent degradation behaviour. This paper aims to explore the technical and economic feasibility of the flexible traction power supply system (FTPSS) integrating ESS and renewable energy sources (RES) based on the traction load characteristics. First, a battery degradation model applicable in its frequent charging and discharging operating conditions is derived. Then this paper develops an operational-sizing co-optimization framework for the ESS in the FTPSS, where the operation decisions are made considering the degradation costs varying with the sizes and energy throughput. To solve this large-scale non-linear intertemporal decision-making problem, an iterative method with a linear programming (LP) core is proposed to achieve the trade-off between computational efficiency and accuracy. The results of the extensive comparative cases show that the proposed approach can achieve approximately 10% higher economic benefits than the existing bi-level sizing strategies for FTPSS.

1 | INTRODUCTION

The electrified railway system, especially high-speed railway, will be exploited more and more in the next future due to its attractive characteristics in terms of costs, environmental pollution, and energy efficiency compared with other transportation methods. However, the tremendous energy consumption and high power demand cannot be ignored with its foreseeable expansion in service frequency and speed of trains [1, 2].

The potential of the energy storage system (ESS) and the renewable energy source (RES) as efficient power conditioners and suppliers has been widely recognized in the smart grid. It also provides an evolutionary path to more sustainable technologies for traction power supply system (TPSS). As a result, the concept of the flexible traction power supply system (FTPSS), which refers to the integration of RES and ESS into the traction grid together with railway power flow controllers to increase system resilience and flexibility, has attracted widespread interest [3, 4].

However, the economic and technical performance of the system is still in doubt and needs to be extensively investigated and evaluated. Specifically, the system can benefit from the reduction of energy consumption and power demand through ESS and RES scheduling. Different from generation resources including RES that have the guaranteed lifetime, however, ESS has the implicit scheduling costs that vary with operating strategy and size due to its degradation characteristics [6]. Therefore, it becomes the main challenge of the problem. This paper aims to maximize the life-cycle benefits by jointly optimizing the sizing and operation strategy of ESS in the presented FTPSS.

In the literature bi-level and single-level optimization frameworks have been described to address the issue. The bi-level optimization framework is generally conducted with operation strategy in the slave layer and system capacity planning in the master layer [7–11]. The rule-based energy management system (EMS) is adopted to control the ESS power based on a defined reference power or bus voltage value in the inner system in [7] and [8]. Based on the above results, the aging characteristic

of ESS is estimated by the semi-experiential method and a battery sizing-oriented cost-benefit analysis is built in the external system. Besides, references [9] and [10] formulate the optimal operation strategy as a mixed integer linear programming (MILP) model in the slave layer, and then evaluate the lifespan of ESS by the rain flow counting method, thus modelling the investment cost in the master layer. A similar bi-level frame is adopted for the sizing of the hybrid energy storage system (HESS) with the state machine-based power flow control strategy and rain flow counting method in [11].

The other approach is to attempt to obtain the sizing and operation strategy in the single-layer optimization problem [12–19]. References [12] and [13] model this joint optimization problem as a convex programming model without considering the effect of ESS degradation. By using the constant degradation rate independent of the ESS operating conditions, the problems are modelled as linear programming (LP) and MILP for different systems, respectively, in [14] and [15]. Reference [16] describes the ESS degradation characteristic as a segmented linear function related to the depth of discharge (DOD) through the introduction of binary variables, and the sizing and energy management model is formulated as MILP and solved by the Dantzig-Wolfe decomposition-based approach. In contrast, a less complex approach is proposed in [17], which introduces a binary variable to represent the switching of the charge/discharge state of the ESS and strictly limits the number of cycles below a predetermined value for any DOD to evaluate the degradation. Especially, based on the properties of the optimized output by a possible heuristic optimization program, references [18] and [19] derive a linear approximation to the degradation function and then place the model internal to the optimization problem.

Despite their insights, few studies have tried to consider the differences between FTPSS and the grid. According to the research on the traction load characteristics in [20], the average frequency of drastic load changes can reach 22 times per hour. Besides, around 95% of the load change events, the peak load reaches above 10.3 MW from an average of 6.24 MW. Different from the slow and subtle dynamics of power flow in the grid, the highly fluctuating and intermittent characteristic of the traction load implies the uncertain and frequent charging and discharging of the ESS. Specifically, the bilevel method does not consider the impacts on the ESS capacity loss and investment cost in the decision-making of ESS charging and discharging actions, and is therefore not accurate enough to assess the life-cycle net economic benefits of FTPSS under the frequent ESS charging and discharging environments. Additionally, the applicability of the MILP constructed from the DOD-based ESS aging model in the single-level framework is limited due to the high computational cost and the unavailability of the necessary variable DOD. Most importantly, neither of the above methods takes into account the impact of traction load characteristics on the grid under the optimized operation strategy of the FTPSS. In general, there mainly exist three challenges for the optimal sizing of ESS in FTPSS.

1. How to derive the applicable ESS degradation models for the intertemporal decisions incorporating short-term operation and life-cycle benefits in the FTPSS.
2. How to quantitatively evaluate and optimize the economic and technical performance of the proposed FTPSS.
3. How to solve the problem including a large set of schedules valid for shorter time periods caused by the fast dynamics in the FTPSS.

In this paper, the structure and mathematical model of the FTPSS are presented grounded on the existing transformer-based TPSS. Instead of simply adopting the existing semi-empirical methods, an accurate and practical batteries (BAT) degradation model considering the capacity and energy throughput is derived to acquire the real-time capacity loss and amortized investment costs based on experimental data. To quantitatively optimize the performance of the FTPSS, an operational-sizing co-optimization framework is established, which takes the proposed economic and load levelling metrics as the objective functions and the operating strategy and sizes of ESS as co-optimized variables. Moreover, this paper proposes an iterative algorithm with the core of LP to solve the formulated non-linear large-scale problem considering the balance of computational efficiency and accuracy. Finally, the quantitative comparisons with conventional TPSS and existing sizing methods show the ability of the proposed method to coordinate the power flow between network-source-load-storage as well as improve the load levelling, economic performance and computational efficiency.

The rest of this paper is organized as follows. The mathematical model of the FTPSS is given in Section 2. Section 3 derives the BAT degradation model. Section 4 outlines the co-optimization framework and the solution approach. The extensive simulations are conducted in Section 5, followed by concluding remarks in Section 6.

2 | MATHEMATICAL MODEL OF FTPSS

The traditional TPSS includes traction transformers, traction networks and trains. Note that discussed TPSS in this paper refers to 27.5-kV AC power supply system for high-speed or heavy-haul railways. To be specific, traction transformers installed in traction substations convert the 220-kV three-phase AC to two separated 27.5-kV single-phase AC from the grid to traction networks. Each power supply section has a different phase from adjacent sections and is hence electrically isolated by the neutral zone. In general, the grid is the only source of traction power for the trains, and the regenerative braking power from the trains is delivered back to the grid.

In order to enable optimal use of energy and reduce the impact of TPSS on grid stability, this paper presents an innovative topology of FTPSS. As shown in Figure 1, a common DC bus acts as an energy hub and connects the end of two adjacent feeding sections, ESS, RES as well as three-phase auxiliary load by multiport energy router composed of DC/AC converters

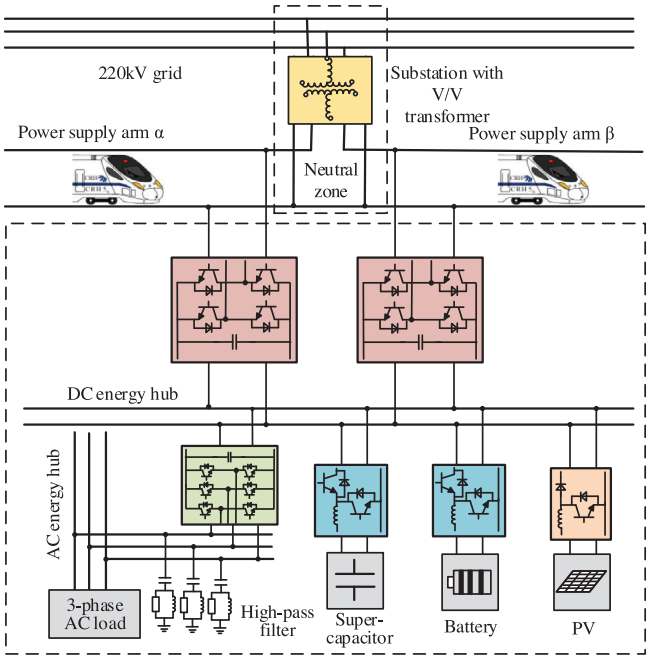

FIGURE 1 The structure of the proposed FTPSS. FTPSS, flexible traction power supply system.

and DC/DC converters. The HESS including battery energy storage system (BESS) and supercapacitors can provide an effective solution for the power regulation of TPSS, which inherits advantages for each individual in terms of power and energy density as well as lifetime [21, 22]. Depending on the geographical location and natural resource of FTPSS, diverse RES can be applied, such as photovoltaics (PV) and wind power systems. For the sake of simplicity, PV is regarded as the representative of RES to explore the possibility of integrating into the TPSS in this paper.

Given the physical network topology, the graph theory provides a visualized and straightforward method to specify the system. The structure of FTPSS is modelled as a directed and connected graph $G = (V; A)$ as shown in Figure 2, where

the set of vertices V models the elements and the edge set A denotes the energy conversion and transmission pathway including converters and transformers in FTPSS. From the energy and topological point of view, there are two types of vertices in the set: vertices with only one inward and outward connection such as consumer vertices ($V_{tr_\alpha}, V_{tr_\beta}$), storage vertices ($V_{bat}, V_{sc}$), RES vertex ($V_{pv}$) and Steiner vertices. The net power flow (NPF) of each branch is defined as the difference between the inward and outward power. For the first type of vertices, the power can be denoted as

$$\begin{aligned} NP\,F_k^{t,\omega} &= PF_{k,\text{ in}}^{t,\omega}/\eta_k - PF_{k,out}^{t,\omega}\eta_k \\ PF_{k,in}^{t,\omega}, PF_{k,\text{ out}}^{t,\omega} &\geq 0,\ \forall t, \omega, k \\ k &\in \{tr_\alpha\ tr_\beta\ sc\ bat\ pv\}. \end{aligned} \tag{1}$$

The Steiner vertices refer to the branch junctions, capable of modelling the two adjacent power supply arms ($V_{ss_\alpha}, V_{ss_\beta}$), the

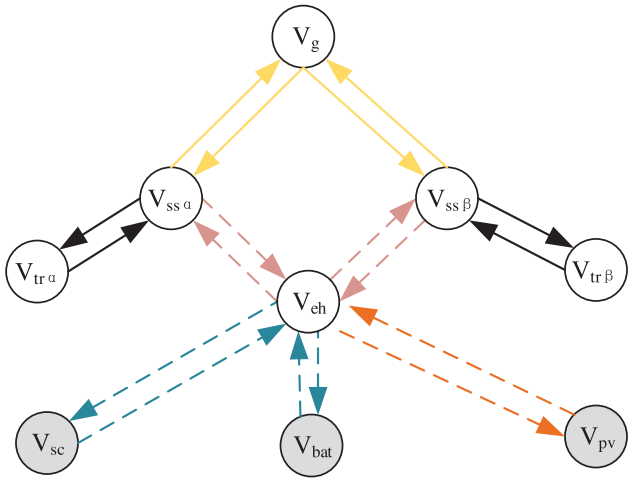

FIGURE 2 The graph representing the physical network topology of FTPSS. Solid lines denote the existed paths for power flow in the traditional TPSS, while dotted lines are additional paths in the proposed FTPSS. TPSS, traction power supply system.

grid (V_g) as well as energy hub (V_{eh}) in this work. The energy balance equations can be formulated by summing the net power of the branches connected to the Steiner vertex to 0 as

$$\begin{aligned} NPF_{ss_\alpha}^{t,\omega} + NPF_{tr_\alpha}^{t,\omega} + NP\,F_{da_\alpha}^{t,\omega} &= 0 \\ NPF_{ss_\beta}^{t,\omega} + NPF_{tr_\beta}^{t,\omega} + NP\,F_{da_\beta}^{t,\omega} &= 0 \\ NPF_{g}^{t,\omega} + NPF_{ss_\alpha}^{t,\omega} + NP\,F_{ss_\beta}^{t,\omega} &= 0 \\ NPF_{da_\alpha}^{t,\omega} + NPF_{da_\beta}^{t,\omega} + NPF_{bat}^{t,\omega} + NPF_{sc}^{t,\omega} + NP\,F_{pv}^{t,\omega} &= 0 \end{aligned} \tag{2}$$

where the subscripts $ss_\alpha, ss_\beta, da_\alpha, da_\beta$ denote the transformer secondary sides and DC/AC converters connected to the power supply arms α and β, and g represents the power grid.

Then a set of constraints with the capacity of branches can be obtained as

$$-P_{dd,sc} \leq NPF_{sc}^{t,\omega} \leq P_{dd,sc} \tag{3}$$

$$-P_{dd,bat} \leq NPF_{bat}^{t,\omega} \leq P_{dd,bat} \tag{4}$$

$$-P_{da_\alpha} \leq NPF_{da_\alpha}^{t,\omega} \leq P_{da_\alpha} \tag{5}$$

$$-P_{da_\beta} \leq NPF_{da_\beta}^{t,\omega} \leq P_{da_\beta} \tag{6}$$

2.1 | Energy characterization

After building the power flow model, we will investigate the energy model of each type of vertex in the rest of this section.

2.1.1 | Traction load

The sum of the single train load can be approximated as the traction load due to the relatively

small short circuit losses in the traction network [23]. The power of the single train can be obtained in the field tests. Another critical factor is the number of trains. Inspired by [20, 24], this work models the time interval between two consecutive trains using the gamma distribution model (μ, σ) based on the analysis of the actual timetables. Then the Monte Carlo sampling method is employed to generate the moments when trains enter and leave the traction arm. We can take the service frequency of trains into account easily by using different μ and σ to generate different loads.

2.1.2 | Storage device

Considering the self-discharge rates, the state-space model related to the current state and action for BAT and SC can be formulated as

$$S_h^{t+1,\omega} = (1-\epsilon_h)\cdot S_h^{t,\omega} + NPF_h^{t,\omega}\cdot \Delta t / E_h^{rate} \quad h \in \{bat,\ sc\}. \tag{7}$$

In order to ensure the HESS operate well, the service conditions are limited to the specific ranges as

$$\begin{aligned} S_h^{\min} \le S_h^{t+1,\omega} \le S_h^{\max} \\ -P_h^{\text{rate}} \le NPF_h^{t,\omega} \le P_h^{\text{rate}} \\ h \in \{\text{bat},\ \text{sc}\} \end{aligned} \tag{8}$$

where state of charge (SOC) of the battery is limited for higher efficiency and less degradation, and SOC limitation of SC considers the step-up capacity of the DC/DC converter.

2.1.3 | PV

The power generated from the PV is mainly determined by the solar radiation intensity and therefore has uncertainties throughout the year. To capture this characteristic, a representative scenario subset ω with the corresponding probabilities π_w is acquired by the scenario reduction technique as described in [8, 24].

The PV generation cannot be fully accommodated by this system due to the intermittence of the traction load. The surplus power of PV either is absorbed by energy storage or discarded, depending on the optimization results. Here $P_{pv}^{t,\omega,\max}$ is defined as the maximum output power of installed PV at time t, and optimal power of PV can be limited as

$$0 \le NPF_{pv}^{t,\omega} \le P_{pv}^{t,\omega,\max} \tag{9}$$

3 | DEGRADATION MODEL OF BESS

Different sized ESS installations can provide different reserve capacities to regulate the load. In turn, the operation strategy of ESS also determines its aging characteristic and indirectly affects the whole life cycle investment cost and the optimal capacity configuration. To be specific, higher ESS usage rates imply larger short-term benefits, but shorter ESS lifetimes. Therefore, a trade-off is supposed to be made between short-term benefits and the ESS value loss by developing the ESS degradation models.

The aging process of SCs is mainly due to parasitic electrochemical reactions and is accelerated in the high-temperature or high-voltage environments [25, 26]. The influence of temperature and external voltage on lifetime is negligible under the control of the storage management system. Therefore, SCs only need to consider the calendar life.

The semi-empirical aging models are formulated to estimate the lifespan of BESS considering the cycling conditions including current rate, temperatures, SOC, DOD and energy throughput in some works [6, 7]. However, such rich details are neither necessary nor practical due to the computational complexity of optimal operation strategy. In the EMS-oriented lifespan estimation of batteries, the characteristic between achievable cycles versus DOD is typically adopted with the rain flow counting algorithm to obtain the lifespan of ESS [9–11]. Nevertheless, the algorithm can only be used as post-assessment methods and applied in the bi-level framework due to the non-convex or non-closed form expression. In other words, the slave layer only optimizes the benefits generated by the operation with its own preferences, without considering the impact on the investment costs in the master layer. This means that the mutually coupled nature of the operation and size selection strategies are not taken into account and therefore the optimality of the results is not guaranteed. There is also some literature that derives the degradation cost as a function of DOD and models the sizing problem as MILP [15, 16]. They may work well with grid applications but become difficult to deal with in the FTPSS because of the introduction of many binary variables and difficult access to DOD.

Therefore, the optimization-oriented degradation model of BESS that can be applied under frequent charging and discharging conditions is developed considering the lifetime determinants. Based on extensive experiments conducted by manufacturers, the conclusion of the aging characteristic normally is revealed in the most typical form of the achievable cycle count (ACC) versus the DOD [30]. It implies that the battery can go through $ACC(D)$ cycles with the DOD equal to D before reaching the end of the lifespan. Therefore, the total energy throughput E_{thp}, the leading cause of the capacity loss, can be calculated as

$$E_{thp}(D) = 2\cdot \eta_{bat}^2 \cdot D \cdot ACC(D)\cdot E_{bat}^{\text{rate}} \tag{10}$$

To express capacity loss per unit energy throughput, we define the average wear coefficient (AWC) as

$$AWC(D) \triangleq (100\% - \zeta\%)\cdot E_{bat}^{rate} / E_{thp}(D) \tag{11}$$

where the battery is regarded to reach the end of the service life when the exploitable energy is below the value $\zeta\%$ of the initial energy E_{bat}^{rate}.

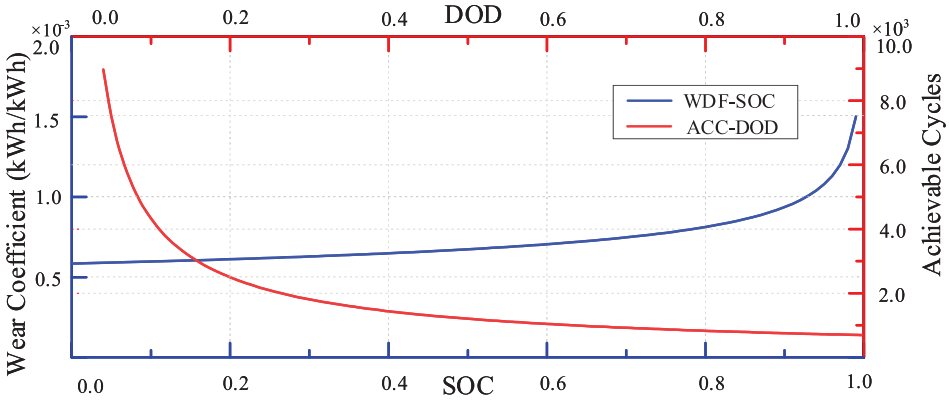

FIGURE 3 An example of ACC-DOD and WDF-SOC curve of a Li-ion battery. ACC, achievable cycle count; DOD, depth of discharge.

A cycle with DOD equal to D means an entire charge–discharge cycle from SOC equal to $(1-D)$ to 1 according to the definition of DOD [31]. Inspired by the definition of probability density function, the wear density function (WDF) is proposed as a function versus SOC, which means that the total capacity loss of a cycle with DOD is the integral of the wear density factor from SOC equal to $(1-D)$ to 1. Hence, AWC can also be expressed by integrating $WDF(S)$ within the corresponding SOC range as

$$AWC(D) = \frac{1}{D} \cdot \int_{1-D}^{1} WDF(S)\, dS \tag{12}$$

Based on (10)–(12), the WDF is deduced as

$$WDF(S) = \frac{1}{2 \cdot \eta_{bat}^2} \cdot \left(-\frac{dACC(D)/dD}{(ACC(D)^2} \right) \tag{13}$$

It is common to fit the ACC-DOD characteristic with the following function:

$$ACC(D) = a \cdot D^{-b} \tag{14}$$

By substituting the above example into (13), the WDF is calculated

$$WDF(S) = \frac{b}{2 \cdot \eta_{bat}^2 \cdot a} \cdot (1-S)^{b-1} \tag{15}$$

An example of ACC-DOD curve of a Li-ion battery is shown in Figure 3 With the curve fitting toolbox in MATLAB, it is reasonable to set $a = 694$ and $b = 0.795$ [32], which is also used in the following case study. The WDF of this type of BESS can be obtained and illustrated in Figure 3. Note that the capacity wear coefficient is dependent on ACC-DOD characteristics, regardless of the specific rated capacities.

To sum up, the capacity loss LS_{bat}^{ω} caused by the charging or discharging process at arbitrary SOC can be evaluated from the following equation. Further, the degraded capacity can be expressed as a cumulative sum by discrete treatment of ΔS. It needs to be pointed out that the SOC change of BESS in a time step is small due to the low ratio between rated power and energy as well as the short sampling time. Thus the approximation is accurate enough.

$$\begin{aligned} LS_{bat}^{\omega} &= \int WDF(S)\, dS \\ &\approx \sum_{t=1}^{T} WDF(S) \cdot \frac{\left| NPF_{bat}^{t,\omega} \right| \cdot \Delta t}{E_{bat}^{\text{rate}}} \\ &\le \frac{(1-\zeta\%)}{T_{bat}} \end{aligned} \tag{16}$$

Instead of using the variation range of SOC, this method uses the SOC and energy throughput at the onset of the charge/discharge action to characterize capacity loss. Firstly, this approach takes into account that the degradation rate is related to the operating conditions and is hence more accurate than using a constant rate. Secondly, it can be integrated into a collaborative optimization framework for the operation and capacity determination of this system, which guarantees the optimality of the solution. Thirdly, it can improve computational efficiency by escaping from introducing a large number of binary variables to record the state of charge/discharge and identify the DOD.

4 | CO-OPTIMIZATION FRAMEWORK

In the above-mentioned bi-level framework, the slave layer only optimizes the benefits generated by the operation with its own preference, without considering the impact on the investment costs in the master layer. However, through the above-derived degradation model of BESS, the capacity and value loss of BESS caused by the operating strategy can be quantified in real time. Therefore, a co-optimization framework is built to obtain the sizing of ESS and operation

strategy of the FTPSS. To be specific, the variables to be optimized include two sets, the power flow strategy $\{NPF_k^{t,\omega}\}$ and sizes$\{P_{dd,bat}, P_{dd,sc}, P_{da_\alpha}, P_{da_\beta}, E_{bat}^{\text{rate}}, E_{sc}^{\text{rate}}, P_{bat}^{\text{rate}}, P_{sc}^{\text{rate}}\}$.

4.1 | Objective function

The objective function to be minimized comprises two parts: (i) the economic cost (F_1) and (ii) load levelling metrics (F_2).

4.1.1 | Economic cost

Because of the frequent scheduling of ESS in the FTPSS, the mutual coupling characteristic between the optimal size during the whole installation period and the daily dispatching of the system needs additional attention. Therefore, one of the sub-objectives F_1 is presented to evaluate the economic performance including the amortized investment cost and operation cost, which can be shown as

$$F_1 = C_{cap} + C_{om} + C_e \tag{17}$$

The specific expressions for these parameters are

$$C_{cap} = \underbrace{\left[C_{dd}\cdot\left(P_{dd,bat}+P_{dd,sc}\right)+C_{da}\cdot\left(P_{da_\alpha}+P_{da_\beta}\right)\right.}_{\text{investment of converters}} + \underbrace{C_{pv}\cdot P_{pv}}_{\text{investment of PV}} + \underbrace{C_{sc}\cdot E_{sc}^{\text{rate}}}_{\text{investment of SC}} + \underbrace{C_{bat}\cdot E_{bat}^{\text{rate}}}_{\text{initial investment of BAT}} + \underbrace{\left.\sum_{N_{rep}} C_{rep}^{bat}\cdot E_{bat}^{\text{rate}}\cdot \text{PVF}\left(r_0, i\cdot T_{bat}\right)\right]}_{\text{replacement cost of BAT}}\cdot\frac{CRF\left(r_0, T_{\text{proj}}\right)}{T_d} \tag{18}$$

$$\text{PVF}\left(r_0, i\cdot T_{bat}\right) = (1+r_0)^{-i\cdot T_{bat}} \tag{19}$$

$$CRF\left(r_0, T_{proj}\right) = \frac{r_0\cdot(1+\mathrm{r}_0)^{\mathrm{T}_{\text{proj}}}}{(1+r_0)^{T_{proj}}-1} \tag{20}$$

$$N_{\text{rep}} = \left\lceil\frac{T_{proj}}{T_{bat}}\right\rceil - 1 \tag{21}$$

$$C_{om} = C_{\text{om bat}}\cdot P_{bat}^{\text{rate}} + C_{om,sc}\cdot P_{sc}^{rate} + C_{om,con}\cdot\left(P_{dd,bat}+P_{dd,sc}+P_{da_\alpha}+P_{da_\beta}\right) \tag{22}$$

$$C_e = \sum_w \pi_w\cdot\left(\sum_t C_p^{t,w}\cdot PF_{g,\text{ out}}^{t,\omega}\cdot\Delta t\right) \tag{23}$$

where C_{cap} is the net present cost of the initial and replacement investment for the system. The present value factor (PVF) is the current value of a future sum of money given a specified rate of return. The capital recovery factor (CRF) gives the present value in terms of the annuity for a given length of time. Through the CRF and PVF, changes in the value of money over time are taken into account. The daily operation and maintenance cost C_{om} is expressed in (22). And C_e is the total electricity bill for railway operators in (23).

4.1.2 | Load levelling

The intermittent traction power surges may not only lead to the voltage flickers in traction net and high demands on infrastructure capacity, but also threaten the safe and reliable operation of the grid. Besides, greater power impulses may occur when only economic factors are considered without limiting the maximum power out of the grid. Unlike the peak shaving in the grid, reducing the maximum peak power is of greater concern and is designed as one of the aims in load levelling.

On the other hand, an additional penalty charge can be levied on the regenerative braking energy fed back into the utility grid due to the nature of stochastic volatility. Utilizing as much regenerative braking energy as possible in the FTPSS can improve energy efficiency and economic benefits.

Based on the above analysis, the load levelling metrics P_{pk} and E_{re} are defined with the infinite norm and 1-norm function as

$$\begin{cases} P_{pk} = \| PF_{g,\text{ out}}^{t,\omega} - P_{thr}\|_\infty \\ \quad = \max\left\{PF_{g,\text{ out}}^{t,\omega} - P_{thr}, 0\right\} \\ E_{re} = \| PF_{g,in}^{t,\omega}\|_1 \\ \quad = \sum_w \pi_w\cdot\sum_t PF_{g,in}^{t,\omega} \end{cases} \tag{24}$$

where P_{pk} is the maximum power greater than the threshold power P_{thr} which is set as the average value of the traction power; while E_{re} is the total regenerative power into the grid. Further, minimizing the load levelling indicator $F_2 = P_{pk} + \alpha\cdot E_{re}$ is presented as the sub-objective in the form of a penalty function, where α is the conversion factor used to adjust the difference in magnitude between the two targets.

4.2 | Problem formulation

There are two main approaches to answer the trade-off question of the two sub-objectives. The first approach, represented by non-dominated sorting genetic algorithm (NSGA)-II optimization techniques, uses the bionic evolutionary algorithms to obtain the Pareto frontier set with the dominant relationship between solutions [33]. However, when it comes to high-dimensional decision variables, this method will make the search space of the evolutionary algorithm grow exponentially and convergence to the optimal solution becomes difficult [34]. The second is to convert the multi-objective optimization model into a single-objective

optimization model by the weighted sum method. Despite sacrificing a certain amount of accuracy and information, it can significantly increase the computational efficiency of this large-scale optimization problem. Hence the objective function is formulated as

$$F = \lambda \cdot F_1 + (1-\lambda) \cdot F_2 \tag{25}$$

By integrating the above sub-objectives (17–24) and the constraints, an operational-planning co-optimization framework for FTPSS can be formulated as

$$\begin{aligned} \mathbf{P1}: \ min \{ & \lambda \cdot \left(\frac{F_1 + (1-\lambda) \cdot \alpha \cdot E_{re}/\lambda - C_{\min}}{C_{\max} - C_{\min}} \right) \\ & + (1-\lambda) \cdot \left(\frac{P_{p\&} - P_{\min}}{P_{\max} - P_{\min}} \right) \} \\ \text{s.t.} \ \ & (1)-(9), (16) \end{aligned} \tag{26}$$

where the value of $((1-\lambda)\cdot\alpha)/\lambda$ is set as the charge per unit of regenerative braking energy into the grid, and λ denotes the weight, the selection of which depends on the needs of the operator and can be guided by the exploration of the impact of the weighting parameters below. While $C_{\max}$ and $P_{\max}$ are indicator values of the original system, $C_{\min}$ and $P_{\min}$ are the minimum values of the sub-objectives calculated by the following proposed algorithm. They are introduced as utopia points and nadir points to normalize the objective functions. The objective consists of two parts according to the magnitude of the sub-objectives: the first two represent the charge and the last represents the maximum peak power.

4.3 | Solution approach

Taking into the computational burden, an iterative frame with the core of an LP optimization problem is proposed. The formulated problem is sequential non-linear programming with large-dimension optimization variables related to the time slot. The non-linearity of **P1** mainly originates from the degradation model of BESS. Specifically, constraint (16) leads to non-linearity and non-convexity of the problem. Therefore, a relaxed version of **P1** is considered by defining the general wear coefficient (GWC) as

$$GWC^{\omega} \triangleq \frac{\sum_t WDF(S) \cdot \left| NPF_{bat}^{t,\omega} \right|}{\sum_t \left| NPF_{bat}^{t,\omega} \right|} \tag{27}$$

By substituting (35) into constraints (16), the non-linear constraint (16) can be transformed as

$$GWC^{\omega} \cdot \sum_t \left| NPF_{bat}^{t,\omega} \right| \cdot \Delta t \le \frac{E_{bat}^{rate}\left(1-\zeta\%\right)}{T_{bat}} \tag{28}$$

With the same objective function and constraints except for (16), the problem **P1** can be transformed as

$$\begin{aligned} \mathbf{P2}: \ min \Bigg\{ & \lambda \cdot \left(\frac{F_1 + (1-\lambda) \cdot \alpha \cdot E_{re}/\lambda - C_{\min}}{C_{\max} - C_{\min}} \right) \\ & + (1-\lambda) \cdot \left(\frac{P_{p\&} - P_{\min}}{P_{\max} - P_{\min}} \right) \Bigg\} \\ \text{s.t.} \ \ & (1)-(9), (28) \end{aligned} \tag{29}$$

Due to the introduction of GWC, the proposed model **P1** develops into LP **P2** that can be solved within polynomial time. Obviously, the value of GWC determines whether the two constraints are equivalent, that is, whether **P1** is equivalent to **P2**. Nevertheless, GWC is determined by the operation strategy of BESS, and the exact value is unknown until the combined size planning and power dispatching optimization problem is solved. Hence, an outer loop is proposed to iterate over GWC, and the update and convergence criterion are formulated in (30) and (31, 32) as

$$GWC^{\omega}(n+1) = \frac{\sum_t WDF(S) \cdot \left| NPF_{bat*}^{t,\omega}(n) \right|}{\sum_t \left| NPF_{bat*}^{t,\omega}(n) \right|} \tag{30}$$

$$\Delta GW\,C^{\omega} = \frac{\left| GWC^{\omega}(n+1) - GWC^{\omega}(n) \right|}{GWC^{\omega}(n)} \le \epsilon \tag{31}$$

$$\Delta F = \frac{\left| F(n) - F^* \right|}{F^*} \le \epsilon \tag{32}$$

where n denotes the n_{th} iteration, the marker $*$ denotes that the variable is the optimal solution in all iterative loops, ΔGWC^{ω} is the the relative change in the value of GWC^{ω} obtained by two consecutive loops, ΔF represents the relative variation between the objective function values obtained in the n_{th} loop and the optimal value of the objective function obtained in all previous loops. The flowchart of the proposed method is shown in Figure 4.

Since the LP problem P2 can always be solved optimally in the inner layer, all constraints of P2 will be satisfied, the conclusion can be drawn as

$$GWC^{\omega}(n) \cdot \sum_t \left| NPF_{bat}^{t,\omega} \right| \cdot \Delta t \le \frac{E_{bat}^{\text{rate}}\left(1-\zeta\%\right)}{T_{bat}} \tag{33}$$

Once the iterative convergence conditions are satisfied, then the relative variation of GWC is less than the given threshold in two consecutive iterations, which is GWC (n + 1) approximate equivalent GWC (n), which follows that:

$$GWC^{\omega}(n+1) \cdot \sum_t \left| NPF_{bat}^{t,\omega} \right| \cdot \Delta t \le \frac{E_{bat}^{\text{rate}}\left(1-\zeta\%\right)}{T_{bat}} \tag{34}$$

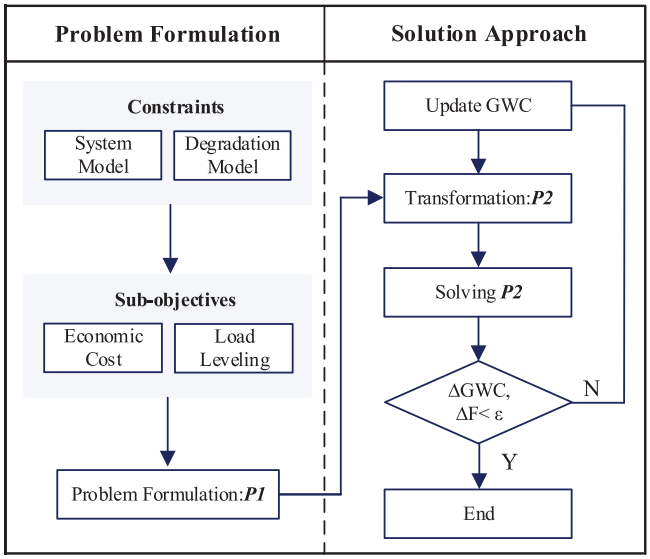

FIGURE 4 The structure of the proposed FTPSS

According to the GWC update criterion, the non-linear constraint (16) holds as follows:

$$\sum_{t} WDF(S) \cdot \left| NPF_{bat}^{t,\omega} \right| \cdot \Delta t \le \frac{E_{bat}^{rate}\left(1-\zeta\%\right)}{T_{bat}} \tag{35}$$

that is, the two constraints (16) and (28), the only difference between P1 and P2, are equivalent. Therefore, as long as the convergence criterions are satisfied, it is guaranteed to find the optimal solution of P1. Through the constants updated in each iteration, the optimal solution of this problem can be found efficiently without significantly compromising the optimality.

5 | CASE STUDY

To verify the effectiveness of the proposed model and method, a simplified FTPSS including PV, HESS, traction load and substations is taken as an example.

5.1 | Simulation parameters

The traction load is demonstrated in Figure 5a, generated with the measured load of the single train and headway modelled by the gamma distribution $\mathcal{G}(1.53,\ 6.94)$. Considering the stochastic nature, the PV outputs are represented by the power profiles of four typical scenarios [9], the magnitudes and probabilities of which are shown in Figure 5b. The specifications of HESS are given in Table 1. BESS module with 1.15 kWh of energy and SC module with 0.15 kWh are adopted as units, the optimal size is expressed with numbers of unit. Besides, a three-level price for the time of use is applied to calculate the electricity bills, which denotes the different prices (0.18 \$/kWh, 0.12 \$/kWh, 0.05 \$/kWh) in peak (12–17), flat (7–12 and 17–22), valley (22–7) periods, respectively.

With regard to the solution procedure, the weight of the economic index is set as 0.9 to highlight the importance of economic benefits. The sampling time is set as the 30 s to capture the dynamics of the system. And the tolerance ε for terminating the loop is set to 1%. The problem is built with the YALMIP toolbox and solved with the GUROBI solver under the MATLAB environment on a computer with Intel Core i7-8700 M CPU at 3.2 GHz and 16 GB RAM.

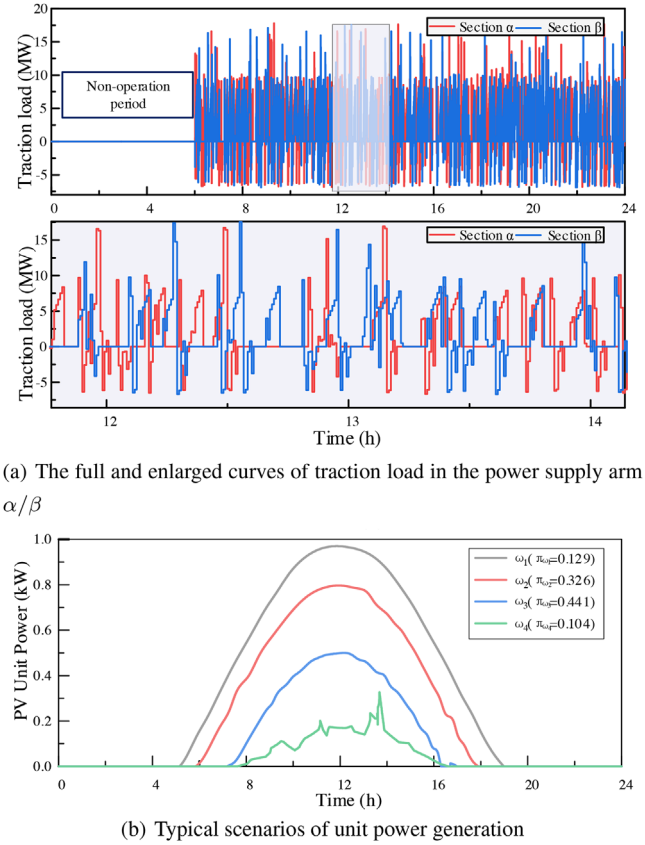

(a) The full and enlarged curves of traction load in the power supply arm α/β

(b) Typical scenarios of unit power generation

FIGURE 5 Simulation parameters

TABLE 1 Parameters of HESS [33, 34]

Parameters	Unit	Batteries	Superca-pacitors
Capital cost	\$/kWh	692	30,800
O&M cost	\$/kW	73	73
Maximum power per unit	kW	4.6	3.375
Energy per unit	kWh	1.15	0.15
Efficiency	–	0.95	0.98
SOC range	–	0.2–0.8	0.25–1
Self-discharge rate	%/day	0.1	20

TABLE 2 Comparison of optimization results for different topologies

Case	PV (kW)	Nu[a]	Nb	Inv ($)[b]	Ene ($)	NPV (%)[c]	Tr (%)	Pk (%)	Re (%)	Pv (%)
Base case	0	0	0	0	7990	0	0	0	0	/
Case1	5000	0	0	548	5600	23.0	21.6	16.4	31.3	53.8
Case2	5000	259	988	1790	4208	24.9	32.8	45.5	67.8	63.8

[a] Nb and Nu are the number of units for batteries and supercapacitors.
[b] Inv and Ene are average daily investment and operation costs.
[c] NPV(%), Tr(%),Pk(%), Re(%) and Pv(%) denote the reduction rate of net present value of daily cost and peak power surge, traction energy consumption as well as the utilization rate of regenerative power and PV output power.

5.2 | Impact of HESS and PV on planning and operation

In order to compare the impact of the HESS and PV, the following three cases are discussed. The comparison of the financial and technical metrics is shown in Table 2.

Base case: Conventional structure of TPSS without any integration of RES and ESS.

Case 1: Two adjacent power supply arms and PV are connected to the DC energy hub.

Case 2: The present topology with optimal sizes obtained by the proposed method.

In Case 1, power can flow between the adjacent supply sections; hence, a third of regenerative braking energy can be absorbed by the trains in traction mode. Besides, more than half of PV output power can be utilized effectively to supply the trains, thus leading to a reduction of about one-fifth of the total traction energy supplied by the grid. Due to the low investment cost of this case, an acceptable net economic benefit can be achieved. However, the peak power is reduced by only 16.4%.

The design of FTPSS in Case 2 significantly diminishes the daily operation cost and therefore yields higher economic profits in spite of the higher investment cost. Moreover, the peak power surge decreases by 45.5% and more than two-thirds of regenerative energy is absorbed and reused due to the best use of bidirectional power transfer capability of HESS achieved by the collaborative optimization of energy management strategy. Besides, the underutilized output of PV is accommodated by HESS, leading to a 10.0% increase in PV utilization rate and a 11.2% curtailment of total traction energy supplied by the grid compared to Case 1.

The optimal energy management strategy is demonstrated in Figure 6. As shown in Figure 6a, compared to the conventional TPSS and PV-only access, the structure and optimization model proposed in this paper significantly reduce the peak power and improve the utilization of regenerative energy, resulting in a smoother power curve, which also implies an increase in infrastructure utilization. For example, the traction powers of Base Case and Case 1 are 23.56 MW and 19.73 MW at 13.15 respectively, and after the improvement of Case 2, the power is 15.19 MW. Besides, the regenerative energy during the periods 12.00 to 17.00 is almost completely absorbed. Combining the power

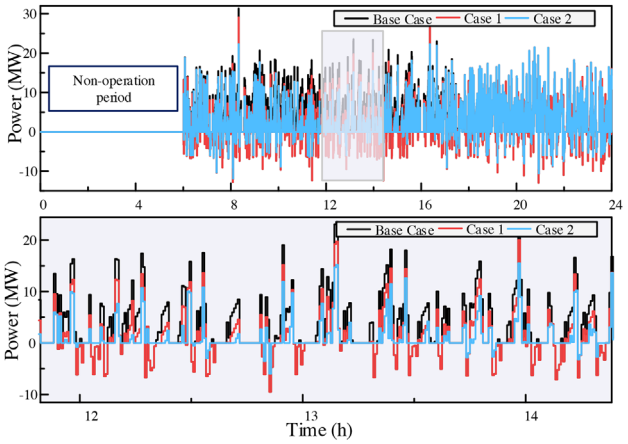

(a) The full and enlarged curves of power flow into/out of the grid under different topologies

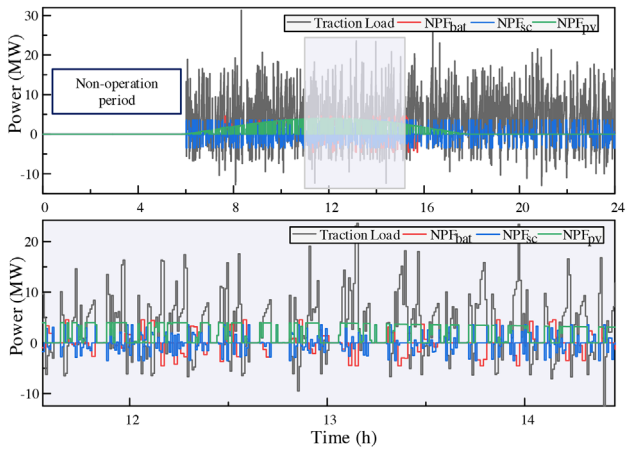

(b) The full and enlarged power flow curves of the presented FTPSS

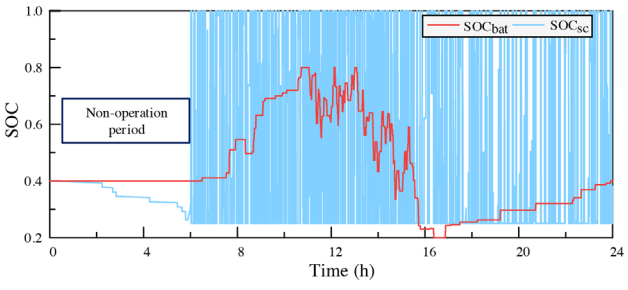

(c) HESS SOC trajectories for the presented FTPSS

FIGURE 6 Comparison of operation strategies under different topologies

TABLE 3 Comparison of optimization results with different weights

Value of λ	Nu	Nb	Inv ($)	Ene ($)	NPV (%)	Tr (%)	Pk (%)	Re (%)	Pv (%)
1	247	787	1718	4264	25.1	31.7	−37.5	64.8	61.6
0.9	259	988	1790	4208	24.9	32.8	45.5	67.8	63.8
0.8	289	1021	1905	4119	24.5	33.7	47.5	70.1	64.8
0.7	318	1296	2186	3877	24.1	35.5	53.5	73.5	69.3
0.6	374	1989	2810	3356	22.8	39.3	67.8	80.5	77.9

TABLE 4 Comparison of different sizing methods for FTPSS

Case	Nu	Nb	Inv ($)	Ene ($)	NPV (%)	Tr (%)	Pk (%)	Re (%)	Pv (%)
Proposed method	259	988	1790	4208	24.9	32.8	45.5	67.8	63.8
Method 1	665	10	2800	3995	14.9	37.3	53.7	81.4	66.9
Method 2	136	1176	1665	3190	39.3	44.3	42.6	92.2	85.3
Method 3	273	0	1209	4813	24.6	29.6	29.8	56.2	60.4

curve of HESS in Figure 6b and the SOC curve of HESS in Figure 6c, it is shown that battery devices store energy in the flat and valley period with a relatively lower electricity price and discharge in the peak period, thus earning more economic benefits. The overall upward trend in the low-price period and downward trend in the high-price period of battery SOC further prove the conclusion. As for SC, it works in the deep charging/discharging active status for most time and plays a critical role in improving the load levelling and economic benefits due to the high power density and almost unlimited charging/discharging cycles. Furthermore, PV has the priority to discharge as the cost-effective energy.

5.3 | Impact of load levelling on planning and operation

The results of cases with different weights are compared to discuss how weights of objectives affect the planning and operation of the system in Table 3. When the weight of economic benefit is set to 1 without any constraint on the power profiles, the cost reduction is mainly derived from the notable conservation of traction energy consumption by regenerative braking energy and the utilization of PV generation. Unfortunately, this setting allows the grid to not only supply power to the trains in traction mode, but also participate in regulating the SOC of the HESS for energy arbitrage, which unsurprisingly results in higher power pulses and more dramatic power fluctuations. As can be seen in Table 3, there is a 37.5% increase in peak power compared to the original load curve. This also demonstrates the need to incorporate load smoothing indices into this co-optimization framework.

The optimal capacities of HESS increase at a super-linear rate as the weight of the load levelling increases. The principal reason is that regulating the drastically fluctuating and high-power traction load requires more reserves. It can be seen that as the investment cost increases, the economic efficiency decreases despite the reduction in operating costs. As expected, the remarkable improvements in traction load profiles and the energy utilization of the PV have been made accordingly. As a matter of fact, dual trade-offs are managed in this sizing problem, including the balance between

investment and return as well as the balance between economic and load smoothing performance. By determining the weight of each index carefully, a compromise of quantity and proportion of two energy storage elements can be gained based on their distinct characteristic and cost.

5.4 | Impact of load levelling on planning and operation

In order to test and verify the necessity of the operational-planning co-optimization framework for the presented FTPSS considering the degradation model of BESS, the popular bi-level frame with the rain flow counting algorithm is adopted as method 1 [9]. Note that the particle swarm optimization algorithm in the master level is used to obtain optimized sizes within the bounds $N_b \in [10, 2000]$ and $N_u \in [10, 800]$. Besides, method 2 and method 3 are given where the battery wear factors are set to 0.00001 and 0.003. The comparisons of the three cases are shown in Table 4 and Figure 7.

In method 1, this framework does not consider the effect of the lifetime in the dynamic operation optimization in the slave level, but only the benefit generated by the participation in the scheduling, then the optimizer always tends to accept the scheduling request for BESS. The capacity loss caused by the over-running of the batteries leads to the high replacement cost and total investment cost. In fact, according to the SOC curve of BESS in Figure 7, the life span is calculated as 0.12 years by rain flow counting algorithm. Therefore, the battery capacity obtained in the bi-level optimization is the minimum value

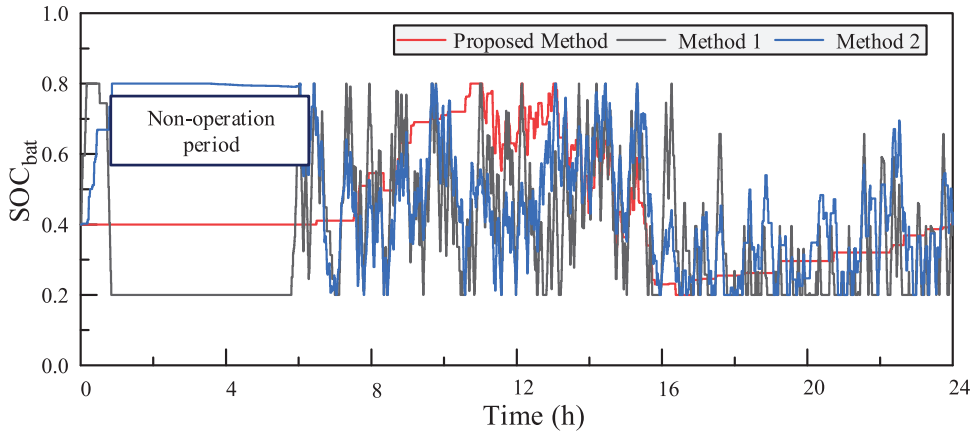

FIGURE 7 BESS SOC trajectories of different sizing strategies. BESS, battery energy storage system.

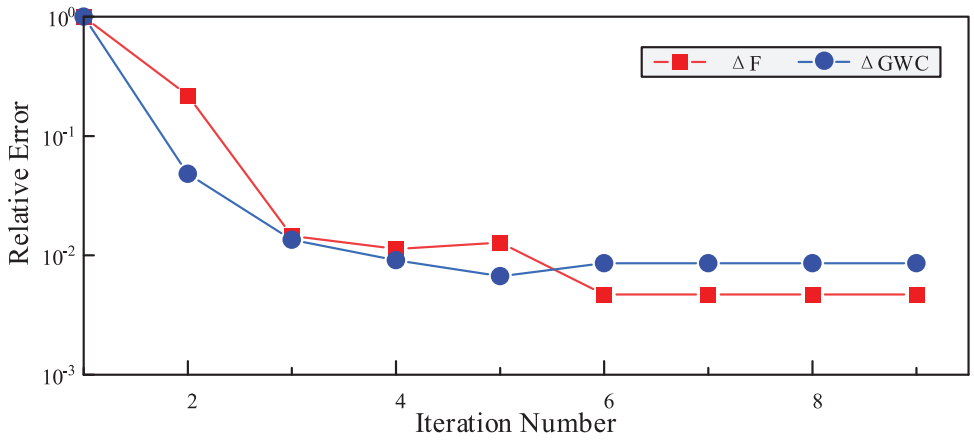

FIGURE 8 Evolution along the iteration number

within the bound. In addition, although the load smoothing can be improved by deploying high-capacity SC, their low energy density leads to limited economic benefits from participating in energy arbitrage.

The actual wear factor of batteries is related to the operating conditions and therefore difficult to acquire. In method 3, the limited energy throughput of BESS hardly creates economic benefits to cover the investment cost, so the optimizer chooses not to configure the batteries in the optimal scheme. In method 2, considering the more significant reserve due to the high energy density of BESS compared to SC, the optimization program tends to use more batteries, so that the unrealistic improvements in both economic and technical indicators occur as the energy throughput increases. Meanwhile, according to the SOC curve in Figure 7, the capacity configuration scheme with underestimated SC size causes BESS to participate not only in energy arbitrage but also in power regulation, which leads to a large SOC operating range and the low lifetime in practice.

Instead, at each moment, the optimizer in the proposed method always weighs the state-related loss in battery value against the benefit of participating in the scheduling, thus ensuring the optimality of the total objective function. As can be seen from the SOC curve in Figure 7, the batteries are charged during the low price period and discharged during the peak price period to maximize the economic benefits.

5.5 | Stability and computational efficiency of the results

The computational efficiency of the proposed method depends on the number of iterations in the external loop and the calculation time of the inner core. The corresponding behaviours of the convergence parameters are shown in Figure 8. The value of the global wear coefficient is stable after four iterations and the target reaches the tolerance in the sixth iteration. The inner solution is attained with the approximate coefficient which is updated with the near-optimal solution in the last round. The mutual guidance between the inner and outer levels renders the algorithm generally able to satisfy the convergence criteria with several rounds. Furthermore, the inner kernel of this problem is modelled as LP with polynomial computation time. Accompanied by the rapid convergence rate as described above,

the presented method is of great superiority in computational efficiency.

6 | CONCLUSION

The aim of this paper is to explore the potential of ESS and RES for TPSS by optimizing the economic and technical performance of the FTPSS. First, a battery degradation model is derived by analyzing the ACC-DOD curves obtained from the experiments. This model relates the degradation cost to the scheduled power and SOC of BESS. Based on the above analysis, a co-optimization framework is developed with investment cost, operation cost and the proposed load smoothing indicators as the optimization objective functions, and the sizes of ESS and the power flow between network-source-load-storage of FTPSS as the optimization variables. What's more, this paper proposes a solution algorithm to achieve the trade-off between accuracy and computational efficiency by outsourcing the non-linear contributions to an external loop and updating the parameters in the inner loop. The results in the case study highlight that the proposed framework is able to capture benefit opportunities better than a traditional bi-level framework, thus achieving roughly 10% higher at the slight sacrifice of load smoothing. Besides, the tradeoff between the economic efficiency and load smoothing metrics is made, which reflects that the dual objective effectively suppresses the increase in peak power. The optimized HESS capacity rises as the demand for power smoothing rises, resulting in a rapid increase in peak smoothing and regenerative energy utilization and a slight decrease in the economy.

The exploration shows that FTPSS with optimally sized devices can be a promising tool in the improvements of the power supply capacity and system stability. Besides, the railway, as one of the largest consumption end users for the grid, can participate in the smart grid programs to create a more environmentally future.

NOMENCLATURE

Indices

ω	Index of scenarios.
k	Index of devices in the system.
t	Index of time.

Parameters

$\epsilon_{bat}, \epsilon_{sc}$	Self-discharge coefficient of batteries (BAT) and supercapacitors (SC).
η_k	Efficiency of device k.
C_{bat}^{rep}	Average daily replacement cost of BAT per unit.
C_{dd}, C_{da}	Average daily investment cost for DC/DC and DC/AC converters per unit.
C_k	Average daily investment cost for device k per unit.
$C_{om,k}$	Average daily operation and maintenance cost for device k per unit.
C_p	Price of energy from the grid.
N_{rep}	Replacement times of BAT.
$P_{pv}^{t,\omega,\max}$	Maximum power for Photovoltaics (PV) during period t for scenarios ω
$S_{bat}^{\max}, S_{sc}^{\max}$	Maximum state of charge (SOC) of BAT/SC.
$S_{bat}^{\min}, S_{sc}^{\min}$	Minimum state of charge of BAT/SC.
T_{bat}	Service period of BAT.
T_d	Number of operation days in a year.
T_{proj}	Service period of the project.

Variables

$NPF_k^{t,\omega}$	Net power flow of device k during period t for scenarios ω
$PF_{k,\text{ in}}^{t,\omega}, PF_{k,\text{ out}}^{t,\omega}$	Power flow into/out of device k during period t for scenarios ω
$E_{bat}^{\text{rate}}, E_{sc}^{\text{rate}}$	Rated energy capacity of BAT/SC.
$P_{bat}^{rate}, P_{sc}^{\text{rate}}$	Rated power capacity of BAT/SC.
$P_{da_\alpha}, P_{da_\beta}$	Rated power of DC/AC converters connecting the DC bus in the traction power supply arm α/β.
$P_{dd,bat}, P_{dd,sc}$	Rated power of DC/DC converters connecting BAT/SC.
$S_{bat}^{t,\omega}, S_{sc}^{t,\omega}$	State of charge of BAT/SC during period t for scenarios ω.

AUTHOR CONTRIBUTIONS

Shanshan Zhang: Conceptualization; Investigation; Methodology; Software; Validation; Visualization; Writing – original draft. Shaobing Yang: Supervision; Writing – review & editing. Qiujiang Liu: Supervision; Writing – review & editing. Bin Hu: Visualization; Writing – review & editing. Junting Zhang: Writing – review & editing.

CONFLICT OF INTEREST

The authors confirm that this article has no conflicts of interest.

DATA AVAILABILITY STATEMENT

The data that support the findings of this study are available from the corresponding author upon reasonable request.

REFERENCES

1. I. UIC: Railway handbook 2017: Energy consumption and co2 emissions. International Energy Agency (IEA) and International Union of Railways (UIC), (2017)
2. Mousavi Gazafrudi S.M., Tabakhpour Langerudy A., Fuchs E.F., AlHaddad K.: Power quality issues in railway electrification: A comprehensive perspective. IEEE Trans. Ind. Electron. 62(5), 3081–3090 (2015)
3. Brenna M., Foiadelli F., Kaleybar H.J.: The evolution of railway power supply systems toward smart microgrids: The concept of the energy hub and integration of distributed energy resources. IEEE Electrification Mag. 8(1), 12–23 (2020)
4. D'Arco S., Piegari L., Tricoli P.: Comparative analysis of topologies to integrate photovoltaic sources in the feeder stations of ac railways. IEEE Trans. Transport. Electrification 4(4), 951–960 (2018)
5. He G., Chen Q., Moutis P., Kar S., Whitacre J.F.: An intertemporal decision framework for electrochemical energy storage management. Nat. Energy 3(5), 404–412 (2018)
6. Yang Y., Li H., Aichhorn A., Zheng J., Greenleaf M.: Sizing strategy of distributed battery storage system with high penetration of photovoltaic

for voltage regulation and peak load shaving. IEEE Trans. Smart Grid 5(2), 982–991 (2013)
7. Shen J., Dusmez S., Khaligh A.: Optimization of sizing and battery cycle life in battery/ultracapacitor hybrid energy storage systems for electric vehicle applications. IEEE Trans. Ind. Informatics 10(4), 2112–2121 (2014)
8. Liu Y., Chen M., Lu S., Chen Y., Li Q.: Optimized sizing and scheduling of hybrid energy storage systems for high-speed railway traction substations. Energies 11(9), 2199 (2018)
9. Zhang Y., Su Y., Wang Z., Liu F., Li C.: Cycle-life-aware optimal sizing of grid-side battery energy storage. IEEE Access 9, 20 179–20 190 (2021)
10. Herrera V.I., Gaztañaga H., Milo A., Saez-de Ibarra A., Etxeberria-Otadui I., Nieva T.: Optimal energy management and sizing of a battery-supercapacitorbased light rail vehicle with a multiobjective approach. IEEE Trans. Ind. Appl. 52(4), 3367–3377 (2016)
11. Baker K., Hug G., Li X.: Energy storage sizing taking into account forecast uncertainties and receding horizon operation. IEEE Trans. Sustainable Energy 8(1), 331–340 (2016)
12. Kargarian A., Hug G., Mohammadi J.: A multi-time scale co-optimization method for sizing of energy storage and fast-ramping generation. IEEE Trans. Sustainable Energy 7(4), 1351–1361 (2016)
13. Sorourifar F., Zavala V.M., Dowling A.W.: Integrated multiscale design, market participation, and replacement strategies for battery energy storage systems. IEEE Trans. Sustain. Energy 11(1), 84–92 (2018)
14. Atia R., Yamada N.: Sizing and analysis of renewable energy and battery systems in residential microgrids. IEEE Trans. Smart Grid 7(3), 1204–1213 (2016)
15. Zhong Z., Zhang Y., Shen H., Li X.: Optimal planning of distributed photovoltaic generation for the traction power supply system of high-speed railway. J. Cleaner Prod. 263, 121394 (2020)
16. De La Torre S., Sánchez-Racero A.J., Aguado J.A., Reyes M., Martínez O.: Optimal sizing of energy storage for regenerative braking in electric railway systems. IEEE Trans. Power Syst. 30(3), 1492–1500 (2014)
17. Foggo B., Yu N.: Improved battery storage valuation through degradation reduction. IEEE Trans. Smart Grid 9(6), 5721–5732 (2017)
18. He G., Chen Q., Kang C., Pinson P., Xia Q.: Optimal bidding strategy of battery storage in power markets considering performance-based regulation and battery cycle life. IEEE Trans. Smart Grid 7(5), 23592367 (2015)
19. Yang S., Song K., Zhu G.: Stochastic process and simulation of traction load for high speed railways. IEEE Access 7, 76049–76060 (2019)
20. Cui G., Luo L., Liang C., Hu S., Li Y., Cao Y., Xie B., Xu J., Zhang Z., Liu Y., et al.: Supercapacitor integrated railway static power conditioner for regenerative braking energy recycling and power quality improvement of high-speed railway system. IEEE Trans. Transp. Electrification 5(3), 702–714 (2019)
21. Bilgin B., Magne P., Malysz P., Yang Y., Pantelic V., Preindl M., Korobkine A., Jiang W., Lawford M., Emadi A.: Making the case for electrified transportation. IEEE Trans. Transp. Electrification 1(1), 4–17 (2015)
22. Liu Q., Wu M., Li J., Yang S.: Frequency-scanning harmonic generator for (inter) harmonic impedance tests and its implementation in actual 2×25kv railway systems. IEEE Trans. Ind. Electron. 68(6), 4801–4811 (2020)
23. Zala L., Modi K., Desai T., Roghelia A.: Headway distribution for NH-8 traffic at Vaghasi village location. In: National Conference on Recent Trends in Engineering & Technology, BVM Engineering College, VV Nagar, Gujarat, India (2011)
24. Aguado J.A., Racero A.J.S., de la Torre S.: Optimal operation of electric railways with renewable energy and electric storage systems. IEEE Trans. Smart Grid 9(2), 993–1001 (2016)
25. Liu Y., Huang Z., Liao H., Lyu C., Zhou Y., Jiao Y., Li H., Hu C., Peng J.: A temperature-suppression charging strategy for supercapacitor stack with lifetime maximization. IEEE Trans. Ind. Appl. 55(6), 6173–6183 (2019)
26. El Mejdoubi A., Oukaour A., Chaoui H., Gualous H., Sabor J., Slamani Y.: Prediction aging model for supercapacitor's calendar life in vehicular applications. IEEE Trans. Veh. Technol. 65(6), 4253–4263 (2016)
27. Suri G., Onori S.: A control-oriented cycle-life model for hybrid electric vehicle lithium-ion batteries. Energy 96, 644–653 (2016)
28. Schneider S.F., Novák P., Kober T.: Rechargeable batteries for simultaneous demand peak shaving and price arbitrage business. IEEE Trans. Sustainable Energy 12(1), 148–157 (2021)
29. Farzin H., Fotuhi-Firuzabad M., Moeini-Aghtaie M.: A practical scheme to involve degradation cost of lithium-ion batteries in vehicle-to-grid applications. IEEE Trans. Sustain. Energy 7(4), 1730–1738 (2016)
30. Zhou C., Qian K., Allan M., Zhou W.: Modeling of the cost of EV battery wear due to v2G application in power systems. IEEE Trans. Energy Convers. 26(4), 1041–1050 (2011)
31. Ye C.-J., Huang M.-X.: Multi-objective optimal power flow considering transient stability based on parallel NSGA-II. IEEE Trans. Power Syst. 30(2), 857–866 (2015)
32. Tian Y., Zhang X., Wang C., Jin Y.: An evolutionary algorithm for large-scale sparse multiobjective optimization problems. IEEE Trans. Evol. Comput. 24(2), 380–393 (2019)
33. Product specification. [online], accessed 2/03/2021 (June 2019). http://www.aowei.com/en/program/productinfo-102-148.html
34. Product specification. online, accessed 2/03/2021 (June 2019). https://www.maxwell.com/products/ltracapacitors/cells

How to cite this article: Zhang, S., Yang, S., Liu, Q., Hu, B., Zhang, J., Guerrero, J.: Sizing and operation co-optimization strategy for flexible traction power supply system. IET Renew. Power Gener. 17, 1329–1341 (2023). https://doi.org/10.1049/rpg2.12626